ADVANCED MATERIALS INTERFACES
www.advmatinterfaces.de

Size-Based Cationic Molecular Sieving through Solid-State Nanochannels

Mubarak Ali, Saima Nasir, Kristina Froehlich, Patricio Ramirez, Javier Cervera, Salvador Mafe, and Wolfgang Ensinger*

The molecular sieving behavior of soft-etched polyimide membranes having negatively charged nanochannels is described experimentally and theoretically using alkali metal–crown ether cationic complexes and alkylammonium cations. To this end, the electrical conduction and current rectification obtained with different alkali electrolyte solutions (LiCl, NaCl, and KCl) and crown ether molecules (12-crown-4, 15-crown-5, and 18-crown-6) are studied. The results suggest that only the $[Li(12C4)]^+$ complex can readily permeate through the nanochannels because significant current decreases are obtained in the cases of the $[Na(15C5)]^+$ and $[K(18C6)]^+$ complexes. In solutions of organic cations ranging from ammonium (NH_4^+) to alkylammonium (R_4N^+) with increasing molecular size, only the smaller ions can conduct high electric currents, suggesting again that the membrane channels are in the nanometer range. Taken together, the observed current decreases and rectification phenomena demonstrate that the functionalized membranes allow a versatile combination of molecular and electrostatic sieving.

1. Introduction

Nanoporous membranes are central to sensing,[1–8] water desalination and filtration,[9–14] and osmotic power generation.[15–23] In most processes, the membrane separates two compartments filled with electrolyte solutions and the transport of molecules or ions through the pores provides the relevant information required for each particular application. This transport is regulated by the channel size and the physico-chemical characteristics of the channel surface. In biological membranes, the high selectivity and fast ion transport achieved are also ascribed to the precise channel size and functional groups distributed along the channel surface.[24–26]

A wide range of experimental techniques are available to tune the channel diameter and surface chemistry to enhance ionic selectivity. They include the preparation of hybrid biological/artificial solid-state membranes,[27,28] channel size tuning through electroless[12,29,30] and atomic layer[31–33] depositions, the grafting of polymer brushes on the channel surface,[34–38] and the deposition of an atomically thin graphene layer on the porous membrane.[39,40] Molecular filtration and discrimination have been achieved using different membranes. For example, Martin and co-workers have employed gold-coated nanochannels for the separation of organic molecules and drug enantiomers based on their charge or molecular size.[12,29,30] Stroeve et al. have demonstrated the pH-responsive transport of ions and biomolecules[41] and Savariar et al. the molecular size-, charge-, and hydrophobicity-based discrimination of organic molecules and proteins[14] using modified nanoporous membranes. Recently, polymer membranes with subnanometer pores have been obtained without specific chemical treatments. For example, track-UV techniques have been employed to fabricate subnanopores which exhibited highly selective and ultrafast ion sieving behavior.[42,43] Moreover, subnanometer pores in metal-organic frameworks integrated inside the bullet-shaped nanochannels of a polymer membrane also exhibited high selectivity towards alkali cations while rejecting divalent ions.[44,45]

Recently, we have developed a soft-etch technique to obtain nanochannels in polyimide (PI) membranes irradiated with heavy ions.[46] PI exhibits high chemical, electrical, and heat resistance. Therefore, the chemical etching of ion tracks in PI membranes requires harsh conditions. Usually, the ion tracks in PI are etched with a strong inorganic etchant (chlorine in hypochlorite) at high temperature. Contrary to chemical etching, in a soft-etching technique, the ion tracked PI membranes are exposed to an organic solvent which selectively dissolves the damage trails (latent tracks) caused by the energetic

Dr. M. Ali, Dr. S. Nasir, K. Froehlich, Prof. W. Ensinger
Department of Material- and Geo-Sciences, Materials Analysis, and Center of Synthetic Biology
Technische Universität Darmstadt
Alarich-Weiss-Str. 02, D-64287 Darmstadt, Germany
E-mail: M.Ali@ma.tu-darmstadt.de, M.Ali@gsi.de

Dr. M. Ali, Dr. S. Nasir
Materials Research Department
GSI Helmholtzzentrum für Schwerionenforschung
Planckstrasse 1, D-64291 Darmstadt, Germany

Prof. P. Ramirez
Departament de Física Aplicada
Universitat Politècnica de València
Valencia E-46022, Spain

Dr. J. Cervera, Prof. S. Mafe
Departament de Física de la Terra i Termodinàmica
Universitat de València
Burjassot E-46100, Spain

The ORCID identification number(s) for the author(s) of this article can be found under https://doi.org/10.1002/admi.202001766.

DOI: 10.1002/admi.202001766

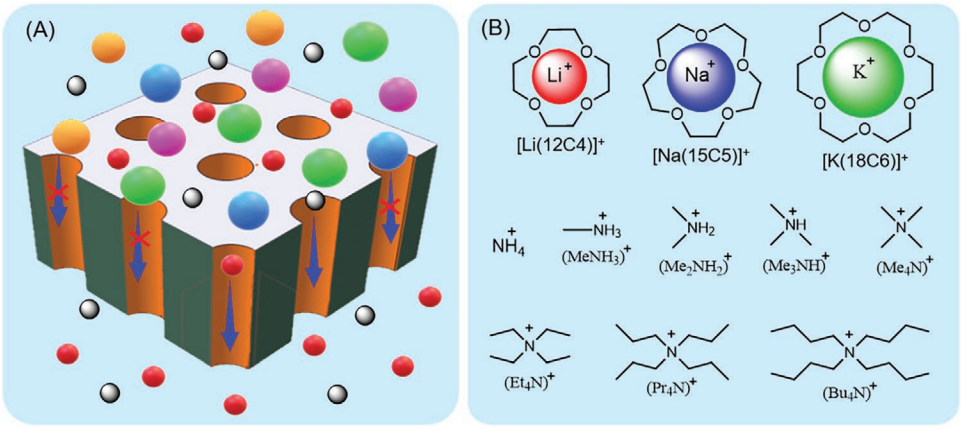

Scheme 1. A) Schematic representation of molecular size-based permeation through the membrane channels and B) the different cationic species used in the experiments.

ion trajectories without affecting the bulk material. The soft-etched membranes allow the passage of ions whose size is smaller than the channel diameter, excluding larger molecules.

We present here an experimental and theoretical analysis of the molecular size-based sieving characteristics of the soft-etched PI membranes. The transport of alkali metal ions, cationic alkali metal-crown ether complexes and alkylammonium cations are studied under an electric potential gradient across the membrane. The resulting ionic and molecular conductions are evaluated from the changes in the transmembrane ion current for a wide range of electrolyte solutions.

2. Results and Discussion

2.1. Experimental Results

We have prepared PI membranes with cylindrical channels in the nanometer range and an areal density of 10^9 pores/cm^2 by means of the soft-etch technique. The latent tracks caused by the heavy ions are dissolved on exposure to dimethylformamide (DMF) solvent without affecting the bulk material. In an effort to characterize these membranes, we study here the conduction and discrimination of cationic alkali metal-crown-ether complexes and alkylammonium cations based on their molecular sizes (**Scheme 1**A,B) under an electric potential gradient. This case constitutes a significant experimental and theoretical extension of our recent work.[45]

2.1.1. Addition of Crown Ethers in Alkali Salt Solutions

Figure 1 shows the current (I)–voltage (V) curves and conductances after the addition of a fixed concentration (25×10^{-3} M) of the crown ethers (12C4, 15C5, and 18C6) in 100×10^{-3} M alkali salt (LiCl, NaCl, and KCl) solutions; see Scheme 1. For the case of LiCl, only small changes in the I–V curves are observed on addition of the crown ethers, contrary to the cases of NaCl and

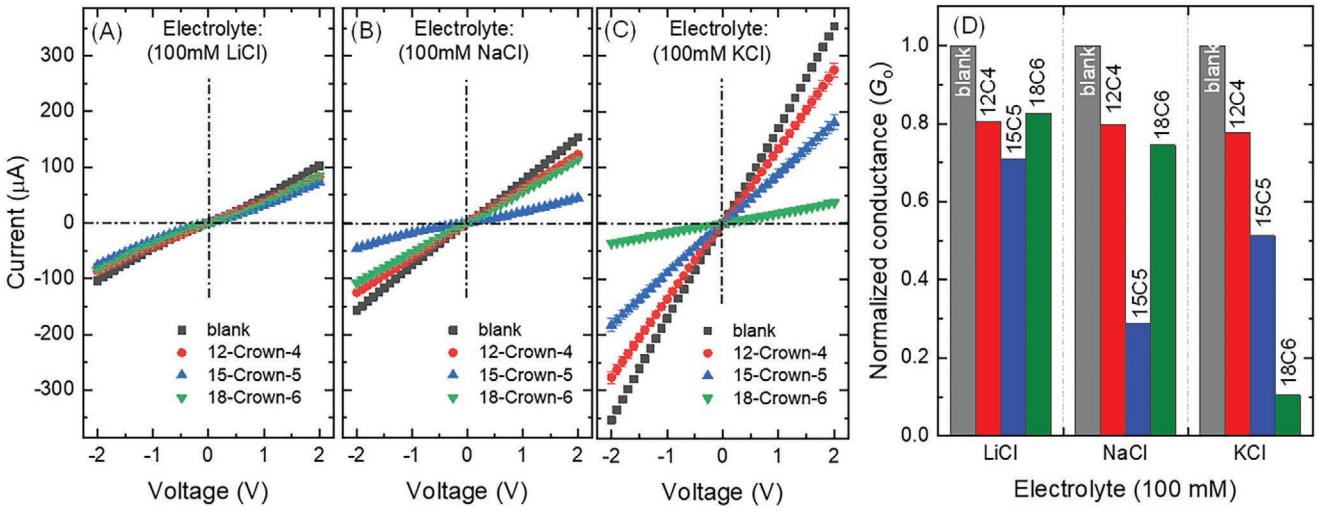

Figure 1. Changes in the I–V curves obtained with the nanoporous membrane after the addition of the different crown ethers at concentration 25×10^{-3} M dissolved in 100×10^{-3} M solutions of A) LiCl, B) NaCl, and C) KCl. D) Changes in the normalized dimensionless conductance obtained from the corresponding I–V curves at 2 V. The blank case makes reference to the absence of crowns in solution.

KCl. It is well known that only Li^+ (effective diameter 0.14 nm) can be accommodated in the cavity of the 12C4 crown ring (0.09–0.12 nm in diameter),[47] forming a positively charged $[Li(12C4)]^+$ complex in solution. Thus, the similar electrical readouts obtained in Figure 1A show that not only the free Li^+ ion but also the $[Li(12C4)]^+$ complex can permeate through the nanochannels, suggesting that the complex size is smaller than the nanochannel diameter. The presence of 15C5 and 18C6 crowns has little influence on the curves because of the inability of these molecules to form complexes with the Li^+ cation.

The case of crown ethers dissolved in NaCl solutions is considered in Figure 1B, Note that the complex formation of 12C4 and 18C6 with Na^+ cation in aqueous solution are negligible.[47–49] Because of the absence of complexation, the *I–V* curves obtained for 12C4 and 18C6 crowns are similar, suggesting that the majority of the current is carried by free Na^+ cations. On the contrary, a significant decrease in the current is noticed for the case of 15C5 molecules. Note that the ionic diameter of Na^+ (0.19 nm) is comparable to the 15C5 ring diameter in the crown ether cavity (0.17–0.22 nm),[47,49] thus allowing $[Na(15C5)]^+$ complexes because of the high stability of the complex (Log $K = 0.7$). Due to the cation-selective membrane, both the Na^+ ion and the $[Na(15C5)]^+$ complex in solution can migrate towards the channel entrance under the applied electric field. However, the $[Na(15C5)]^+$ complexes cannot enter the channel in this case, leading to a significant current decrease in the corresponding *I–V* curve of Figure 1B. This observation suggests that the channel diameter should be close to the effective size of the $[Na(15C5)]^+$ complex. The crystallographic data show that the approximate outer diameter of the $[Na(15C5)]^+$ complex molecule is ≈0.81 nm.[50]

Figure 1C considers the KCl case where the stability constant of K^+ cation with 12C4 crown is almost negligible while for 15C5 and 18C6 it is ≈0.7 and ≈2.06, respectively.[47–49] For the 15C5 crown, however, a noticeable current decrease occurs. Although the cation size is larger than the crown ether cavity diameter, the formation of a (2:1) sandwich $[K(15C5)_2]^+$ complex can still take place,[51–53] which could explain the change in the *I–V* curve. For the 18C6 crown, the drastic decrease in ionic current is observed which clearly suggests the formation of $[K(18C6)]^+$ complexes in solution because of the compatibility between the K^+ cation diameter (0.27 nm) and the cavity size (0.26–0.32 nm) of the 18-crown-6 molecule.[47–49] It was not possible to quantitatively determine the aperture size from direct imaging of the nanochannels but these results are suggestive of a nanochannel diameter larger than the $[Li(12C4)]^+$ but of the order of the $[K(18C6)]^+$ complex size, which could explain the apparent channel blockage experienced by those K^+ ions that are not in complexed form.

Figure 1D shows the changes observed in the normalized membrane conductance after the different crown ethers addition. These electrical conductances are obtained at 2 V from the corresponding *I–V* curves of Figures 1A–C and suggest that only the $[Li(12C4)]^+$ complex can pass through the nanochannels without interfering the uncomplexed Li^+ ions for the case of LiCl (a small conductance decrease is observed compared to the blank case). For the NaCl case, however, the 15C5 crown leads to a 71% reduction in the conductance. For KCl, the formation of $[K(15C5)_2]^+$ and $[K(18C6)]^+$ complexes gives 50% and 90% decreases in the conductance, respectively.[47,49] Moreover, Figure S1, Supporting Information, suggests that the decrease of the membrane current is due to the partial obstruction of the pore opening caused by the formation of cationic metal-crown complexes when compared with the changes in the bulk solution conductivity upon the addition of different crown ethers in the corresponding alkali electrolyte solution. In addition to soft-etched nanoporous membranes, we have also performed a control experiment under the same set of electrolyte solutions using a single conical nanopore in PI membrane. As expected, the addition of crown ethers in the electrolyte solutions (Figure S2, Supporting Information) and tetra-alkylammonium chlorides (Figure S3, Supporting Information) only lead to minor changes in the corresponding *I–V* curves associated with the bulk solution conductivity decrease. Note that the tip opening of the cone is large enough to allow the free permeation of metal-crown complexes and R_4N^+ cations across the membrane under the applied potential.

Figure 2 shows the effect of the crown ether concentration on the membrane conductance. For the case of LiCl, the increase in

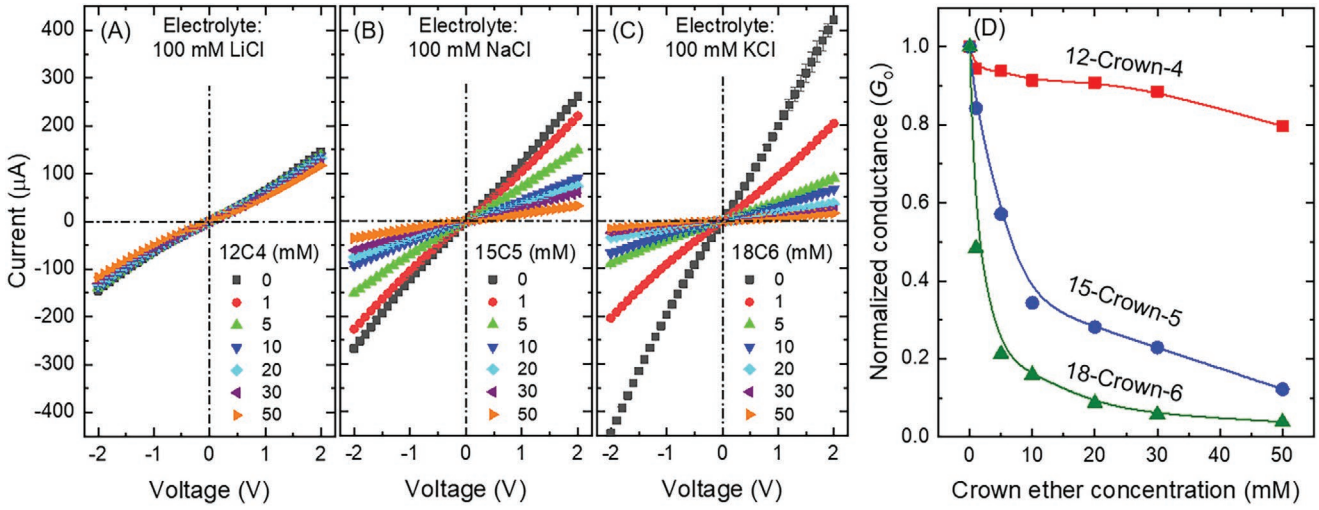

Figure 2. A–C) Effect of the crown ether concentration on the *I–V* curves of alkali metal chloride solutions under symmetric electrolyte conditions. D) The normalized conductances obtained from the corresponding *I–V* curves.

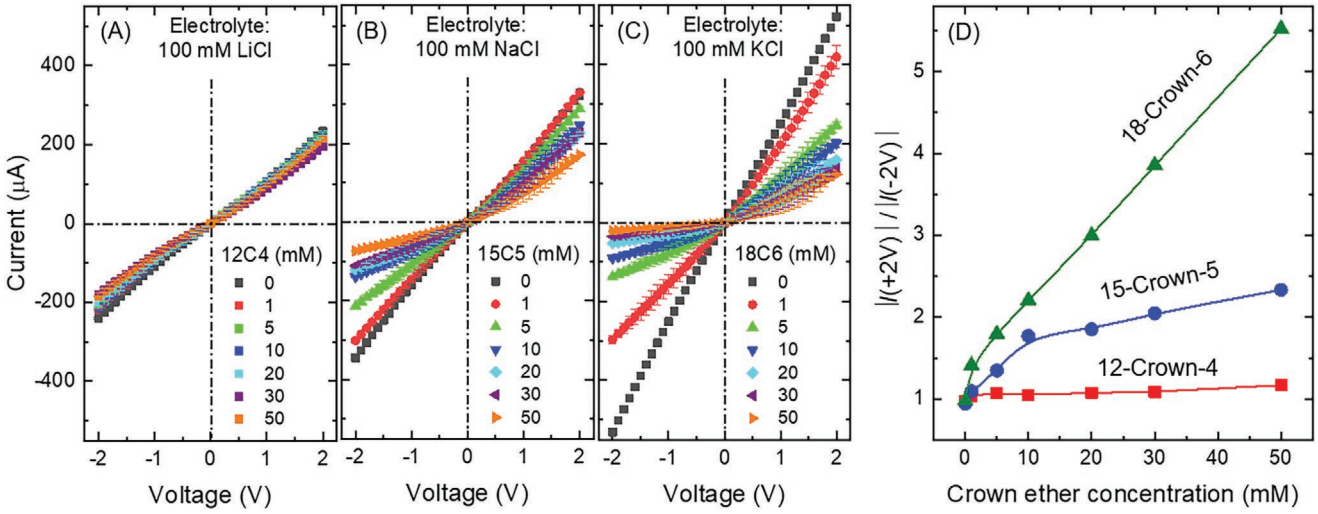

Figure 3. The effect of crown ether concentrations on the *I–V* curves measured with alkali metal chloride solutions under asymmetrical conditions in the left and right external solutions bathing the membrane. One side of the membrane (working electrode, WE) is exposed to a metal chloride solution while the other side (ground electrode, GE) is in contact with A–C) different crown ether concentrations prepared in the corresponding electrolyte solutions. D) The electric current rectification ratios obtained from the corresponding *I–V* curves.

the 12C4 crown concentration could not induce major changes in the *I–V* curve, suggesting translocation of both Li^+ free ions and $[Li(12C4)]^+$complexes across the membrane (Figure 2A). On the contrary, increasing the 15C5 and 18C6 crown concentrations leads to significant current decreases for NaCl and KCl (Figures 2B and 2C).

Figure 2D quantifies the conductance decreases obtained with increasing the crown ether concentration. Again, the results strongly suggest that the formation of complexes with different molecular sizes in the background electrolyte solution modulates the transport through the nanoporous membrane. In particular, the conductance decreases could be ascribed to: 1) the inability of the large cationic $[Na(15C5)]^+$ and $[K(18C6)]^+$ complexes to translocate through the nanochannels and 2) the strong electrostatic interaction of the $[Na(15C5)]^+$ and $[K(18C6)]^+$ complexes with the negatively charged channel entrance causing a partial channel blocking and increased hindrance for the incoming Na^+ and K^+ free ions. By increasing the crown ether concentration, both effects become more marked because of the decrease in the number of non-complexed free cations crossing the membrane and the increase in the number of complexed cations causing the mentioned partial channel blocking and increased hindrance due to the reduced effective area for transport.

Figures 3A–C considers the case of an asymmetrical crown ether addition, as opposed to the symmetric case of Figures 2A–C. To this end, one side of the membrane is exposed to the blank (100×10^{-3} M) alkali metal chloride solutions while the other side is in contact with different crown ether concentrations in the corresponding solutions. For the case of the LiCl/12C4 combination, only small changes in the current with no rectification are observed when increasing the 12C4 crown concentration because the cationic $[Li(12C4)]^+$ complexes can translocate through the channels without interfering with the Li^+ free ions transport (Figure 3A).

For the NaCl/15C5 and KCl/18C6 combinations, however, Figures 3B and 3C show both current decreases and rectification phenomena. Note that the uncomplexed Na^+ and K^+ ions pass through the channel at positive voltage while the $[Na(15C5)]^+$ and $[K(18C6)]^+$ complexes cannot proceed through the channel at negative voltage. This fact leads to the current rectification shown in Figure 3D which follows a monotonous increase with the 15C5 and 18C6 crown concentration. As expected, this effect is more pronounced for $[K(18C6)]^+$ (≈1.15 nm) than for $[Na(15C5)]^+$ (≈0.81 nm) because of the different molecular sizes.[50,54] The experimental fact that the rectification ratio does not depend on the 12C4 crown concentration which shows that the $[Li(12C4)]^+$ complex is conducted across the membrane. Again, this result suggests that the effective channel diameter should be higher than the $[Li(12C4)]^+$ complex size but in the range of the $[Na(15C5)]^+$ and $[K(18C6)]^+$ complex diameters.

To better understand the complexation phenomena as well as the electrostatic interactions of the positively charged metal–crown ether complexes with the negative channel charges, we have also measured the *I–V* curves of concentrated KCl solutions (**Figures 4**A,B). To this end, a fixed concentration (25×10^{-3} M) of the 18C6 crown is used in different concentrations (0.1, 0.5, and 1 M) of KCl. In confined geometries, an effective screening of the surface charges by the mobile counter ions occurs at high enough electrolyte concentrations. In addition, the number of non-complexed free ions increases with the salt concentration. These effects lead to the increase of the normalized conductance with the KCl concentration shown in Figure 4C. Indeed, the formation of $[K(18C6)]^+$ complexes in 0.1, 0.5, and 1 M KCl solutions lead to decreases of 77%, 67%, and 56% in the membrane conductance of Figure 3C compared to that of the crown-free solution.

2.1.2. Addition of Alkylammonium Cations in Ammonium Salt Solution

We have also considered the effects of organic cations in **Figures 5**A–H using two series of alkylammonium chloride

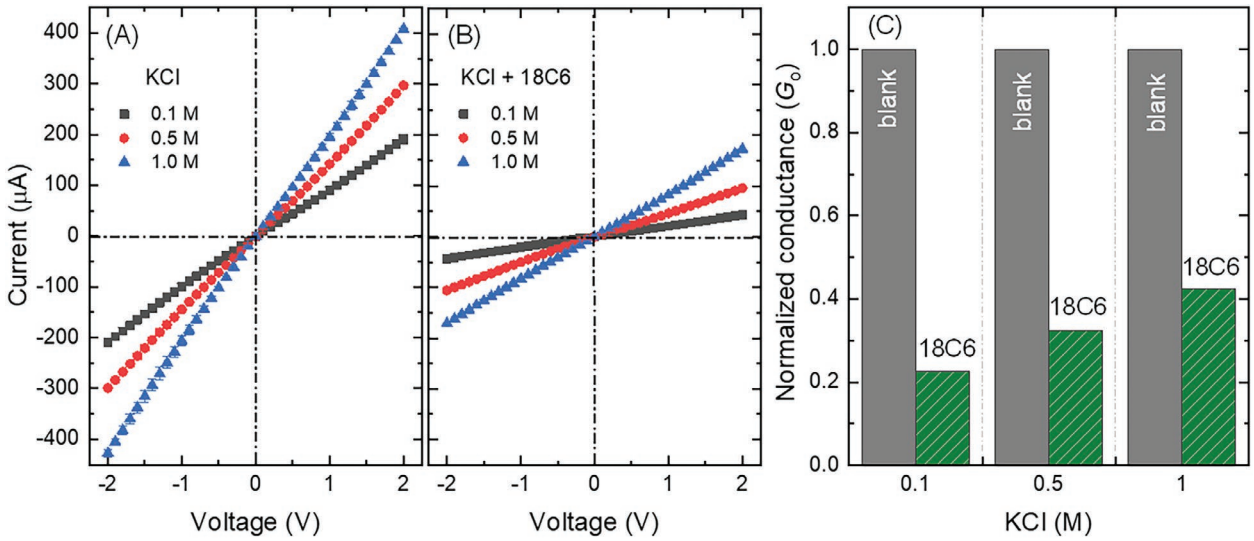

Figure 4. The *I–V* curves of the membrane A) before and B) after the addition of 25×10^{-3} M 18C6 crown ether for different KCl concentrations. C) The normalized conductance obtained from the corresponding *I–V* curves before and after adding the crown ether.

salts with different molecular sizes:[55,56] *i*) the ammonium (NH_4^+) cation derivatives with successive methyl group substitution, that is, methylammonium ($MeNH_3^+$), dimethylammonium ($Me_2NH_2^+$), trimethylammonium (Me_3NH^+), and tetramethylammonium (Me_4N^+) cations; and *ii*) the quaternary ammonium (R_4N^+) cations in which the methyl groups of Me_4N^+ are replaced by ethyl-, propyl- and butyl- chains, that is, tetraethylammonium (Et_4N^+), tetrapropylammonium (Pr_4N^+), and tetrabutylammonium (Bu_4N^+) cations. The electrolyte solutions used to examine the organic cation current reductions have different mole fractions of alkylammonium chloride/ammonium chloride at a constant total concentration of cation and anion, that is, $[RNCl + NH_4Cl] = 100 \times 10^{-3}$ M.

The *I–V* curves of Figures 5A–D correspond to electrolyte solutions having different mole fractions of methylated-ammonium derivatives and ammonium cations ($Me_nNH_m^+/NH_4^+$, $n + m = 4$). For the case of $MeNH_3^+$ /NH_4^+, no significant changes in the ion current with increasing the concentration of $MeNH_3^+$ cations in the electrolyte solution are observed. This fact suggests that the diameters of the two cations, NH_4^+ (0.33 nm) and $MeNH_3^+$ (0.37 nm) present in the electrolyte solution are smaller than the channel diameter. For the case of di-, tri-, and tetra-methylated-ammonium cations, however, the current decreases significantly with the mole fraction, suggesting that these bulky cations translocate much more slowly than the ammonium ion under the applied potential. When the electrolyte solution contains only di-, tri-, and tetra-methylated-ammonium cations (mole fraction = 1.0), the current and conductance (Figure 5H) reductions depend markedly on the size of the corresponding cations. Figure 5H shows that replacing NH_4^+ by $MeNH_3^+$ (0.37 nm), $Me_2NH_2^+$ (0.47 nm), Me_3NH^+ (0.51 nm), and Me_4N^+ (0.55 nm) leads to 26%, 54%, 78%, and 90% reductions in the conductance, respectively. Although this significant conductance decrease suggests that the Me_4N^+ cation might have an effective size of the order of the nanochannel diameter, the fact is that not only molecular size but also hydrophobic effects could influence translocation.

To check further the above results, we have considered other quaternary ammonium ions larger than the Me_4N^+ cations in Figures 5E–G where electrolyte solutions with different R_4N^+/NH_4^+ cation mole fractions are used under symmetric conditions. Et_4N^+ exhibits a trend similar to that of Me_4N^+ at low mole fractions with a ≈15% drop in the current. On the contrary, the bulky cations Pr_4N^+ and Bu_4N^+ cations give a sudden current drop (≈50%) at low mole fractions (Figure 5H). For mole fractions over 0.1, both Pr_4N^+ (≈0.9 nm) and Bu_4N^+ (≈1.0 nm) virtually block the pores, suggesting that their sizes could be commensurate with the channel opening diameter. While we could not accurately determine the channel size from imaging techniques and carried out a complete electrochemical characterization instead, the above facts provide an indirect but reasonable estimation of the effective membrane pore radii.

Figures 6A–H consider the asymmetric case where electrolyte solutions of different alkylammonium cation mole fractions are added on one side of the membrane while the other side contains ammonium chloride solutions. As expected, the asymmetric addition of $MeNH_3^+$ cation does not induce any noticeable change in the current at positive ($V > 0$) or negative ($V < 0$) voltages. In this case, $MeNH_3^+$ can pass through the nanochannel when $V < 0$ without any hindrance because the cation size is smaller than the nanochannel diameter. For the other ammonium cations, a successive decrease in the current is noticed as the number of methyl substitution increases in the ammonium cation. This current decrease is more marked when the methyl groups of Me_4N^+ are substituted with longer chain alkyl groups, that is, ethyl (Et), propyl (Pr), and butyl (Bu) moieties. As expected, the current decrease is more pronounced at $V < 0$ than at $V > 0$, leading to a current rectification that increases with the cation size (Figure 6H).

The transmembrane current decrease and rectification phenomena observed in metal crown complexes and organic cations (Figures 1–6) have some resemblances to the blocking processes that occur in the ion channels of biological membranes in the presence of bulky ions.[57] Similarly, we have

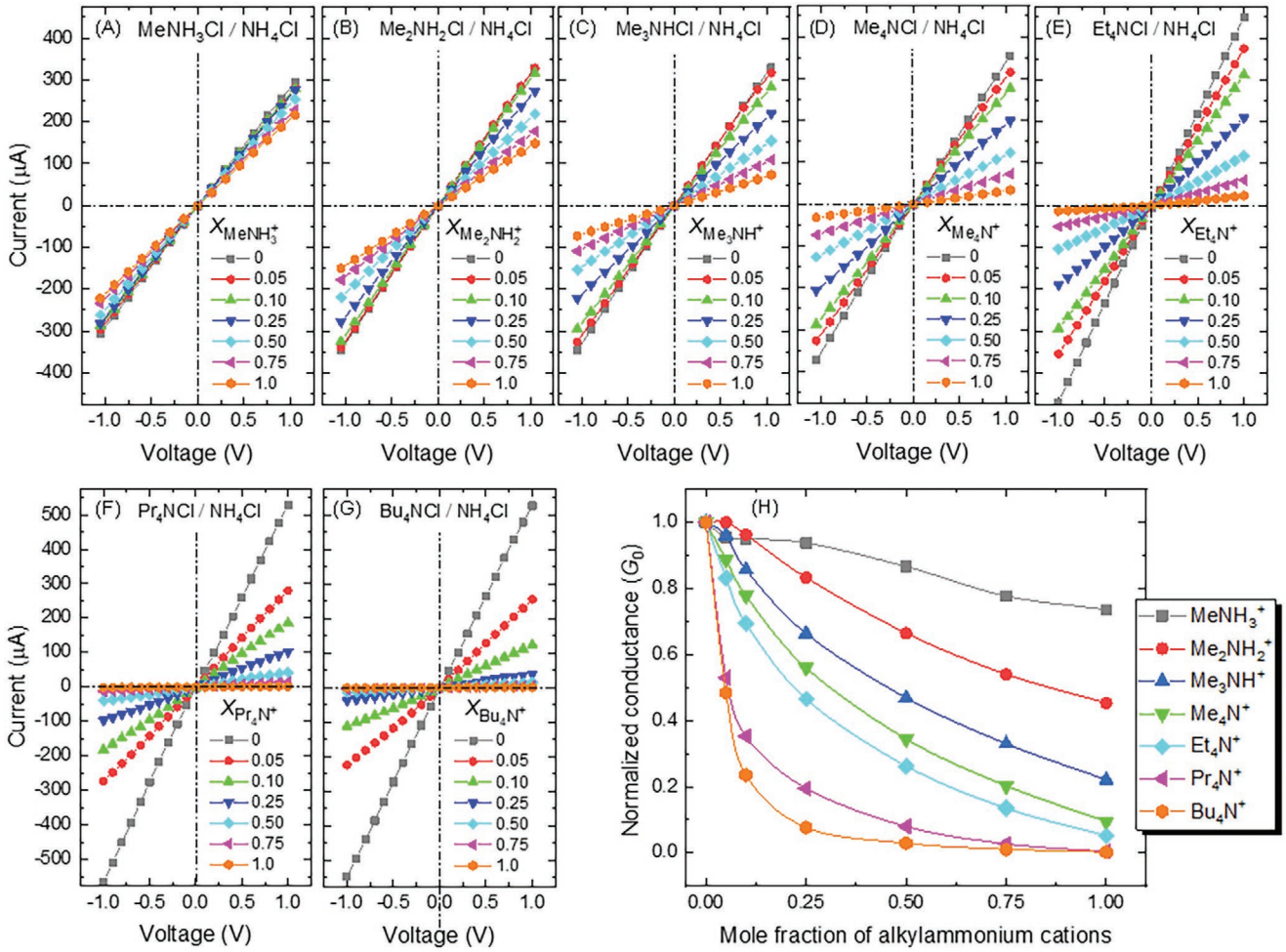

Figure 5. A–G) The *I–V* curves for different mole fractions of alkylammonium cations in NH_4Cl solutions. H) The normalized conductance obtained from the corresponding *I–V* curves as a function of the mole fractions.

studied the rectification characteristics and current blockage of cylindrical nanochannels asymmetrically exposed to electrolyte solutions containing oppositely charged nanoparticles whose sizes were larger than the channel diameter.[58,59] The channel entrance and blocking mechanisms associated with the current blockage in biological channels exposed to antibiotic molecules and ionic drugs have also been discussed.[60,61] A previous study by Martin and coworkers have also described that the presence of the 18C6 in solution exert effects on the ionic current for the different case of a conical channel when the tip opening is comparable to the effective crown ether size.[54] In particular, the rectification phenomena associated with the addition of the 18C6 under asymmetric conditions in a single channel membrane have been described with much detail.[54]

2.2. Theoretical Results

The experimental data by Martin and coworkers[54] were interpreted using a model based on the liquid junction established at the external solution/membrane interface and the different transference numbers of the $[K(18C6)]^+$ complex in the solution and the conical channel entrance. In addition to the comprehensive experimental characterization of the ionic conduction through the nanoporous membrane using different crown ethers and ions, we have developed a different model that allows a qualitative description of the effects associated with the cationic complex formation constant K, the crown ether total concentration c_{LT}, and the salt concentration c_S in Figures 2D, 4C, and 5H. Although the model makes reference to the KCl salt, it can be readily extended to other cases.

Crown ethers complex cations are because of the lone pairs on the ether oxygen atoms.[54] The model used here introduces the complex formation equations:

$$K = \frac{c_{L+}}{c_+ c_L} \tag{1}$$

$$c_L + c_{L+} = c_{LT} \tag{2}$$

where c_+ is the cation concentration c_L is the crown ether concentration, and c_{L+} is the cationic complex concentration. The

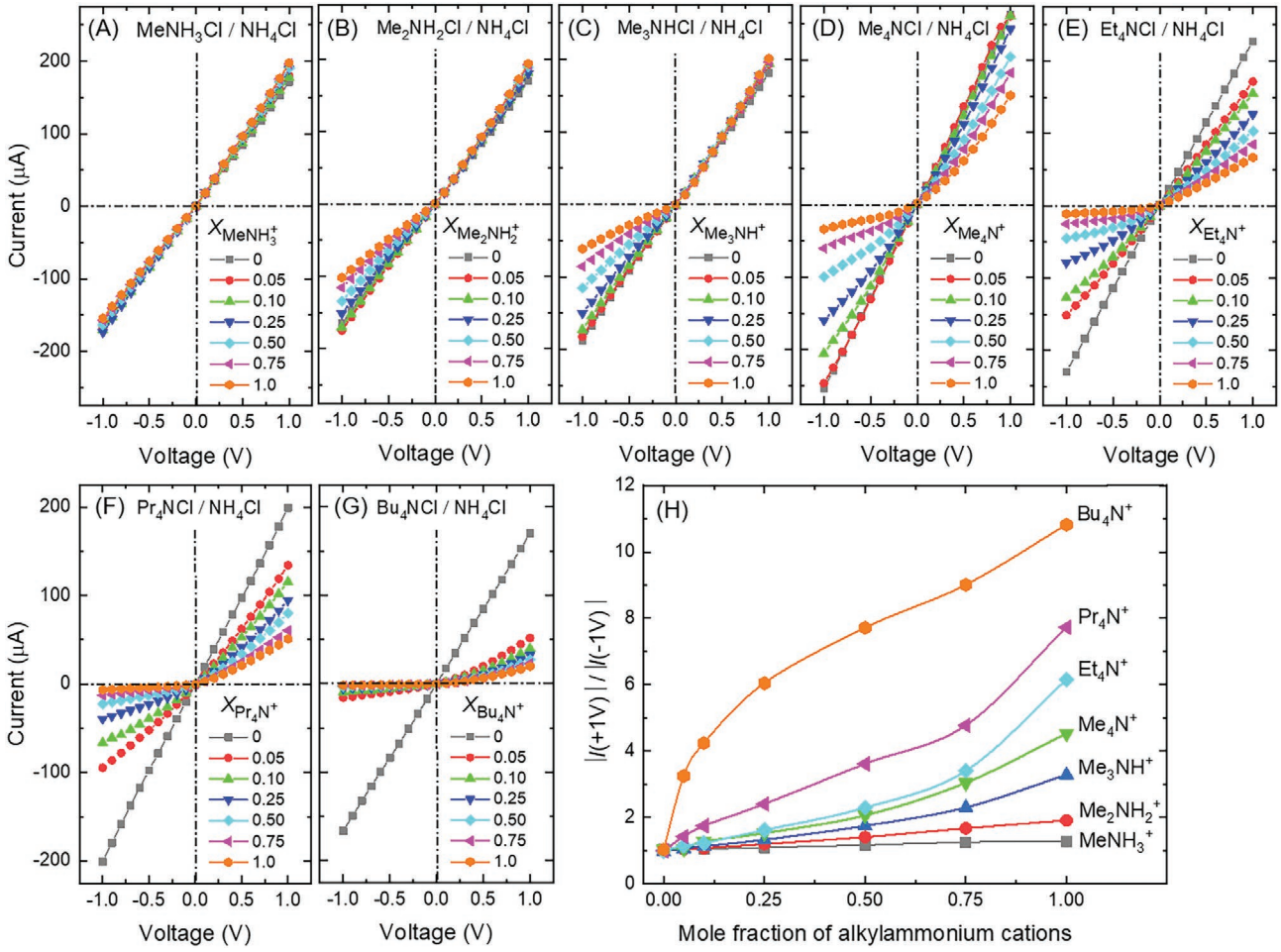

Figure 6. A–G) The *I–V* curves for different mole fractions of alkylammonium cations in NH_4Cl solutions under asymmetric electrolyte conditions. One side of the membrane (working electrode, WE) is exposed to a 100×10^{-3} M NH_4Cl solution while the other side (ground electrode, GE) is exposed to different alkylammonium mole fractions with [NH_4Cl + RNCl] = 100×10^{-3} M. F) The rectification ratios obtained from the corresponding *I–V* curves as a function of the mole fractions.

ionic concentrations are coupled by the electroneutrality equation in the external solution:

$$c_{L+} + c_+ = c_- \tag{3}$$

where the anion concentration is equal to the salt concentration, $c_- = c_S$. Equations (1)–(3) can be solved to give:

$$c_+ = \frac{-\left[1 - K(c_S - c_{LT})\right] + \sqrt{\left[1 - K(c_S - c_{LT})\right]^2 + 4Kc_S}}{2K} \tag{4}$$

$$c_L = \frac{c_{LT}}{1 + Kc_+} \tag{5}$$

$$c_{L+} = Kc_+c_L \tag{6}$$

The ionic concentrations in the membrane solution, which are denoted by overbars here, can be obtained in terms of Equations (4)–(6) and the Donnan potential drop ϕ_D through the solution/membrane interface[62] as:

$$\bar{c}_+ = c_+ \exp(-\phi_D) \tag{7}$$

$$\bar{c}_{L+} = c_{L+} \exp(-\phi_D) \tag{8}$$

$$\bar{c}_- = c_S \exp(\phi_D) \tag{9}$$

where $\phi_D < 0$ for a negative channel charge[63,64] is expressed in RT/F units, being R, F, and T the gas constant, the Faraday constant, and the temperature, respectively. Equations (7)–(9) are coupled by the electroneutrality equation in the membrane channel solution:

$$c_+ \exp(-\phi_D) + c_{L+} \exp(-\phi_D) = c_S \exp(\phi_D) + X \tag{10}$$

where X denotes the membrane fixed charge concentration, which is typically in the range 0.1–1 M for these channels.[63] Equation (10) can be solved for ϕ_D to give:

$$\phi_D = -\ln\left[\frac{X}{2c_S} + \sqrt{\left(\frac{X}{2c_S}\right)^2 + \left(\frac{c_+ + c_{L+}}{c_S}\right)}\right] \tag{11}$$

In order to omit the unknown channel geometry characteristics, we introduce the normalized conductance ratio of Figures 2D and 4C:

$$G_0 = \frac{G}{G_{\text{blank}}} = \left(\frac{1}{1+\bar{c}_{L+}/c_{LT,0}}\right) \frac{D_+\bar{c}_+ + D_{L+}\bar{c}_{L+} + D_-\bar{c}_-}{D_+\left[\frac{X}{2}+\sqrt{\left(\frac{X}{2}\right)^2+c_S{}^2}\right]+D_-\left[-\frac{X}{2}+\sqrt{\left(\frac{X}{2}\right)^2+c_S{}^2}\right]} \quad (12)$$

where G_{blank} is the membrane conductance G in absence of ether crown ($c_{LT} = 0$) and D_i (i = +, L+, −) are the ion diffusion coefficients. A number of factors may lead to the conductance reduction observed experimentally including channel blocking[64] and decreased surface mobility.[65] The phenomenological approach used for the conductance of Equation (12) includes a pre-factor smaller than unity to account for these factors. In particular, the experimental fact that both the cationic complex and the channel radius are in the nanometer range is suggestive of a complex concentration-dependent channel occlusion and hindrance.[60,61] This factor contains a reference blocking concentration $c_{LT,0} = 25 \times 10^{-3}$ M which corresponds to the ether crown concentration used in the experiments. As a first approximation, we assume that $D_+ = D_- = 2\times10^{-9}\ \text{m}^2\ \text{s}^{-1}$, which corresponds to the KCl case and takes $D_{L+} \approx 0$ because of the partial channel blocking and significant hindrance experienced by the cationic complex. Note that the typical experimental current $I = 100$ μA of Figure 1C obtained at a voltage $V = 1$ V can be approximately described by using the equation $I \approx N_p\pi r^2F^2D_+XV/(RTd)$ where $N_p = 10^9$ pores, $d = 12$ μm is the membrane thickness, and r is the channel radius.[63] Introducing the above values for I, N_p, D_+, X, V, and d, the channel radius r is found to be in the nanometer range, consistent with the partial channel blocking and hindrance assumption.[60,61]

Equation (12) allows an approximate description of the effects of K and c_{LT} at constant c_S (**Figure 7**A) and of c_S at constants K and c_{LT} (Figure 7B). While the simplifying assumptions introduced in the model preclude a direct comparison between theory and experiment, the results of Figures 7A and 7B are in qualitative agreement with the experimental data of Figures 2D and 4C for the experimental values of c_{LT} and c_S used here. As to the values of K, we emphasize that formation constants of the order of $1/(10 \times 10^{-3}\ \text{M}) = 100\ \text{M}^{-1}$ are reasonable and have been previously used for the potassium cation complexed by 18C6 in aqueous solution.[54] On the contrary, the formation constant should be very small for the case of the uncomplexed Li^+ ion and 18C6. These experimental facts give support to the range of values used for K in Figure 7A. Previous experimental and theoretical work concerning the carrier-mediated transport of alkali cations and neutral species concerning crown-ethers and liquid membranes can be found in refs. [66,67].

Note also that the experimental rectifications of Figure 3D could also be qualitatively described by using a directional channel blocking and decreased mobility model for the Na^+ and K^+ ions (Figures 3B and 3C), which should occur only at $V < 0$ for the asymmetric conditions employed in the external solutions. In particular, the conductance measured at −2 V is low compared with that obtained at +2 V (Figure 3D) because the electric field imposed through the membrane acts to enhance the partial channel blocking by the complexed cation when the ground electrode solution is exposed to the 18C6 crown. These directional ionic conduction phenomena can be incorporated in the theoretical description when the complex concentration $\bar{c}_{L+}$ in Equation (12) is made to depend on the sign of the applied potential that would shift the equilibrium potential $\phi_D < 0$ in Equation (8) to more negative electric potentials, as explained in previous models developed for conical nanochannels and ion channels.[63,64]

3. Conclusion

We have studied experimentally and theoretically the electrostatic and molecular size-based sieving obtained with

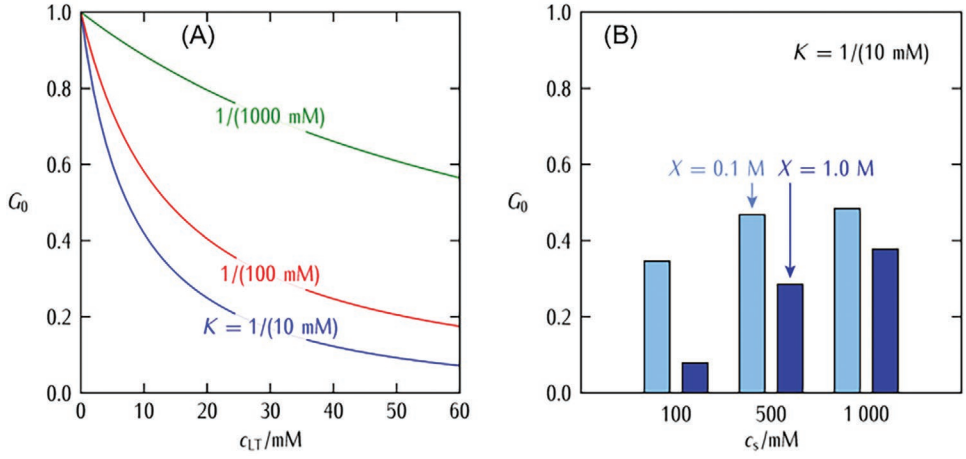

Figure 7. A) Normalized conductance $G_0 = G/G_{blank}$ as a function of the crown ether concentration c_{LT} obtained with Equation (12) for the membrane fixed charge concentration $X = 0.3$ M and the different formation constants shown in the curves. B) G_0 as a function of the salt concentration c_S for the formation constant $K = 1/(10 \times 10^{-3}\ \text{M}) = 100\ \text{M}^{-1}$ and the two fixed charge concentrations shown in the bars. The model can give a qualitative description of the experimental data using reasonable values for the system parameters.

a soft-etched PI membrane. To this end, the electrical conduction and current rectification of alkali metal-crown ether complexes and alkylammonium ions is investigated under a wide range of experimental conditions. The results suggest that relatively small cationic species such as the alkali ions, the ammonium ion, and the $[Li(12C4)]^+$ complex can be translocated across the membrane under an applied voltage. On the contrary, the negatively charged nanochannels could not allow the passage of bigger cationic molecules whose sizes are in the nanometer scale. Note however that not only the geometrical size but also the particular hydrophobicity could influence translocation and pore hindrance.

4. Experimental Section

Chemicals: The chemicals include lithium chloride (LiCl, ≥99.0%), sodium chloride, (NaCl, ≥99.9%), potassium chloride (KCl, ≥99.0%), 12-crown-4 (12C4, 98%), 15-crown-5 (15C5, 98%), 18-crown-6 (18C6, ≥99.0%), ammonium chloride (NH_4Cl, ≥99.5%), methylammonium chloride ($MeNH_3Cl$, ≥99.0%), dimethylammonium chloride (Me_2NH_2Cl, ≥98.0%), trimethylammonium chloride (Me_3NHCl, ≥98.0%), tetramethylammonium chloride (Me_4NCl, ≥98.0%), tetraethylammonium chloride (Et_4NCl, ≥98%), tetrapropylammonium chloride (Pr_4Cl, 98.0%), tetrabutylammonium chloride (Bu_4NCl, ≥97.0%), and DMF (99.8%) were purchased from Sigma-Aldrich, Schnelldorf, Germany, and used without further purification.

Soft-Etching of Latent Ion Tracks: The heavy ion irradiation of 12 µm thick polyimide membrane (Kapton50 HN, DuPont;) was carried out at the linear accelerator UNILAC (GSI Helmholtz Centre for Heavy Ion Research, Darmstadt, Germany). Polymer samples were irradiated using the swift heavy ions (Au) of energy 8.6 MeV per nucleon with an ion fluence of 10^9 ions/cm^2. Then, the latent ion tracks in the PI membrane were activated by UV light (320 nm, 3h) irradiation on both sides. To transform the ion-tracks into nanochannels, the UV-activated PI membranes were exposed to DMF solvent for 24 h at room temperature. Finally, the DMF-treated samples were thoroughly washed with distilled water before electrical measurements. Additional details can be found elsewhere[46] where the authors considered the transport of alkali and small organic cations only.

Current–Voltage (I–V) Curves: For the measurement of electrical readout, the DMF-treated membrane sample was mounted between the two compartments of a home-made electrochemical cell.[15,46] The effective membrane area in contact with the electrolyte solution was ≈8 mm^2. The electrolytes containing various crown-ether concentrations were prepared in aqueous alkali chloride (100×10^{-3} M) solutions. The electrolyte solutions of various alkylammonium cations were prepared in 100×10^{-3} M aqueous solution of ammonium chloride. The *I–V* curves were recorded with a Keithley 6487 picoammeter (Keithley Instruments, Cleveland, Ohio). For this purpose, the Ag|AgCl electrodes were dipped in the electrolyte solution on both sides of membrane sample to control the input potentials and output currents in a triangular wave signal.[15,46]

Supporting Information

Supporting Information is available from the Wiley Online Library or from the author.

Acknowledgements

P.R., J.C., and S.M. acknowledge the funding from project PGC2018-097359-B-I00, Ministerio de Ciencia e Innovación. K.F., M.A., S.N., and W.E. acknowledge the support from the LOEWE project iNAPO, Hessen State Ministry of Higher Education, Research, and the Arts, Germany. The authors are thankful to Prof. C. Trautmann and Dr. E. Toimil Molares (GSI, Material Research Department) for their support with the heavy ion irradiation experiments and Mr. E. Schubert for the designing of electrochemical cells. The heavy ion irradiation is based on a UMAT experiment, which was performed at the X0-beamline of the UNILAC at the GSI Helmholtzzentrum fuer Schwerionenforschung, Darmstadt (Germany) in the frame of FAIR Phase-0.

Open access funding enabled and organized by Projekt DEAL.

Conflict of Interest

The authors declare no conflict of interest.

Data Availability Statement

Research data are not shared.

Keywords

alkylammonium cations, ionic conduction, metal ion-crown ether complexes, molecular sieving, polyimide membranes

Received: October 7, 2020
Revised: December 23, 2020
Published online: February 8, 2021

[1] M. Ali, R. Neumann, W. Ensinger, *ACS Nano* **2010**, *4*, 7267.
[2] M. Ali, P. Ramirez, I. Duznovic, S. Nasir, S. Mafe, W. Ensinger, *Colloids Surf., B* **2017**, *150*, 201.
[3] M. Ali, M. N. Tahir, Z. Siwy, R. Neumann, W. Tremel, W. Ensinger, *Anal. Chem.* **2011**, *83*, 1673.
[4] H. Bayley, P. S. Cremer, *Nature* **2001**, *413*, 226.
[5] K. Healy, B. Schiedt, A. P. Morrison, *Nanomedicine* **2007**, *2*, 875.
[6] A. de la Escosura-Muñiz, A. Merkoçi, *ACS Nano* **2012**, *6*, 7556.
[7] S. Nasir, M. Ali, I. Ahmed, C. M. Niemeyer, W. Ensinger, *ChemPlusChem* **2020**, *85*, 587.
[8] K. Zhan, Z. Li, J. Chen, Y. Hou, J. Zhang, R. Sun, Z. Bu, L. Wang, M. Wang, X. Chen, X. Hou, *Nano Today* **2020**, *33*, 100868.
[9] X. Hou, W. Guo, L. Jiang, *Chem. Soc. Rev.* **2011**, *40*, 2385.
[10] X. Hou, H. C. Zhang, L. Jiang, *Angew. Chem., Int. Ed.* **2012**, *51*, 5296.
[11] S. B. Lee, D. T. Mitchell, L. Trofin, T. K. Nevanen, H. Soderlund, C. R. Martin, *Science* **2002**, *296*, 2198.
[12] C. R. Martin, Z. Siwy, *Nat. Mater.* **2004**, *3*, 284.
[13] S. Nasir, P. Ramirez, M. Ali, I. Ahmed, L. Fruk, S. Mafe, W. Ensinger, *J. Chem. Phys.* **2013**, *138*, 034709.
[14] E. N. Savariar, K. Krishnamoorthy, S. Thayumanavan, *Nat. Nanotechnol.* **2008**, *3*, 112.
[15] P. Ramirez, J. Cervera, V. Gomez, M. Ali, S. Nasir, W. Ensinger, S. Mafe, *Small* **2018**, *14*, 1702252.
[16] P. Ramirez, V. Gomez, J. Cervera, S. Nasir, M. Ali, W. Ensinger, S. Mafe, *Nano Energy* **2015**, *16*, 375.
[17] Y. Feng, W. Zhu, W. Guo, L. Jiang, *Adv. Mater.* **2017**, *29*, 1702773.
[18] K. Xiao, P. Giusto, L. P. Wen, L. Jiang, M. Antonietti, *Angew. Chem., Int. Ed.* **2018**, *57*, 10123.
[19] G. Laucirica, A. G. Albesa, M. E. Toimil-Molares, C. Trautmann, W. A. Marmisollé, O. Azzaroni, *Nano Energy* **2020**, *71*, 104612.
[20] J. Kim, S. J. Kim, D.-K. Kim, *Energy* **2013**, *51*, 413.
[21] S. Balme, T. Ma, E. Balanzat, J.-M. Janot, *J. Membr. Sci.* **2017**, *544*, 18.

[22] Y. Zhu, K. Zhan, X. Hou, *ACS Nano* **2018**, *12*, 908.
[23] J. Zhang, K. Zhan, S. Wang, X. Hou, *Soft Matter* **2020**, *16*, 2915.
[24] B. Hille, *Ionic Channels of Excitable Membranes*, Sinauer Associates Inc., Sunderland, MA **2001**.
[25] T. Luo, S. Abdu, M. Wessling, *J. Membr. Sci.* **2018**, *555*, 429.
[26] Z. Zhu, D. Wang, Y. Tian, L. Jiang, *J. Am. Chem. Soc.* **2019**, *141*, 8658.
[27] S. Balme, J. M. Janot, L. Berardo, F. Henn, D. Bonhenry, S. Kraszewski, F. Picaud, C. Ramseyer, *Nano Lett.* **2011**, *11*, 712.
[28] S. Balme, F. Picaud, S. Kraszewski, P. Déjardin, J. M. Janot, M. Lepoitevin, J. Capomanes, C. Ramseyer, F. Henn, *Nanoscale* **2013**, *5*, 3961.
[29] C. R. Martin, M. Nishizawa, K. Jirage, M. S. Kang, S. B. Lee, *Adv. Mater.* **2001**, *13*, 1351.
[30] K. B. Jirage, J. C. Hulteen, C. R. Martin, *Science* **1997**, *278*, 655.
[31] A. Spende, N. Sobel, M. Lukas, R. Zierold, J. C. Riedl, L. Gura, I. Schubert, J. M. M. Moreno, K. Nielsch, B. Stühn, C. Hess, C. Trautmann, M. E. Toimil-Molares, *Nanotechnology* **2015**, *26*, 335301.
[32] P. Chen, T. Mitsui, D. B. Farmer, J. Golovchenko, R. G. Gordon, D. Branton, *Nano Lett.* **2004**, *4*, 1333.
[33] C.-M. Wang, D.-L. Kong, Q. Chen, J.-M. Xue, *Front. Mater. Sci.* **2013**, *7*, 335.
[34] W. Guo, H. W. Xia, L. X. Cao, F. Xia, S. T. Wang, G. Z. Zhang, Y. L. Song, Y. G. Wang, L. Jiang, D. B. Zhu, *Adv. Funct. Mater.* **2010**, *20*, 3561.
[35] S. Nasir, M. Ali, W. Ensinger, *Nanotechnology* **2012**, *23*, 225502.
[36] G. Pérez-Mitta, J. S. Tuninetti, W. Knoll, C. Trautmann, M. E. Toimil-Molares, O. Azzaroni, *J. Am. Chem. Soc.* **2015**, *137*, 6011.
[37] M. Tagliazucchi, I. Szleifer, *Soft Matter* **2012**, *8*, 7292.
[38] B. Yameen, M. Ali, R. Neumann, W. Ensinger, W. Knoll, O. Azzaroni, *Nano Lett.* **2009**, *9*, 2788.
[39] Y. Fu, X. Guo, Y. Wang, X. Wang, J. Xue, *Nano Energy* **2019**, *57*, 783.
[40] W. Li, L. Liang, S. Zhao, S. Zhang, J. Xue, *J. Appl. Phys.* **2013**, *114*, 234304.
[41] P. Stroeve, N. Ileri, *Trends Biotechnol.* **2011**, *29*, 259.
[42] Q. Wen, D. Yan, F. Liu, M. Wang, Y. Ling, P. Wang, P. Kluth, D. Schauries, C. Trautmann, P. Apel, W. Guo, G. Xiao, J. Liu, J. Xue, Y. Wang, *Adv. Funct. Mater.* **2016**, *26*, 5796.
[43] P. Wang, M. Wang, F. Liu, S. Ding, X. Wang, G. Du, J. Liu, P. Apel, P. Kluth, C. Trautmann, Y. Wang, *Nat. Commun.* **2018**, *9*, 569.
[44] J. Lu, H. Zhang, J. Hou, X. Li, X. Hu, Y. Hu, C. D. Easton, Q. Li, C. Sun, A. W. Thornton, M. R. Hill, X. Zhang, G. Jiang, J. Z. Liu, A. J. Hill, B. D. Freeman, L. Jiang, H. Wang, *Nat. Mater.* **2020**, *19*, 767.
[45] X. Li, H. Zhang, H. Yu, J. Xia, Y.-B. Zhu, H.-A. Wu, J. Hou, J. Lu, R. Ou, C. D. Easton, C. Selomulya, M. R. Hill, L. Jiang, H. Wang, *Adv. Mater.* **2020**, *32*, 2001777.
[46] K. Froehlich, S. Nasir, M. Ali, P. Ramirez, J. Cervera, S. Mafe, W. Ensinger, *J. Membr. Sci.* **2020**, *617*, 118633.
[47] H. Høiland, J. A. Ringseth, T. S. Brun, *J. Solution Chem.* **1979**, *8*, 779.
[48] H. K. Frensdorff, *J. Am. Chem. Soc.* **1971**, *93*, 600.
[49] R. M. Izatt, J. S. Bradshaw, S. A. Nielsen, J. D. Lamb, J. J. Christensen, D. Sen, *Chem. Rev.* **1985**, *85*, 271.
[50] G. W. Buchanan, M. Gerzain, C. Bensimon, *Acta Crystallogr., Sect. C: Struct. Chem.* **1994**, *50*, 1016.
[51] H.-R. Yu, J.-Q. Hu, X.-H. Lu, X.-J. Ju, Z. Liu, R. Xie, W. Wang, L.-Y. Chu, *J. Phys. Chem. B* **2015**, *119*, 1696.
[52] S. Flink, B. A. Boukamp, A. van den Berg, F. C. J. M. van Veggel, D. N. Reinhoudt, *J. Am. Chem. Soc.* **1998**, *120*, 4652.
[53] S.-Y. Lin, S.-W. Liu, C.-M. Lin, C.-h. Chen, *Anal. Chem.* **2002**, *74*, 330.
[54] E. A. Heins, L. A. Baker, Z. S. Siwy, M. Mota, C. R. Martin, *J. Phys. Chem. B* **2005**, *109*, 18400.
[55] A. Villarroel, N. Burnashev, B. Sakmann, *Biophys. J.* **1995**, *68*, 866.
[56] E. R. Nightingale, *J. Phys. Chem.* **1959**, *63*, 1381.
[57] B. Hille, *Ion Channels of Excitable Membranes*, Sinauer Associates Inc., Cary, NC **2001**.
[58] M. Ali, P. Ramirez, S. Nasir, Q.-H. Nguyen, W. Ensinger, S. Mafe, *Nanoscale* **2014**, *6*, 10740.
[59] M. Ali, P. Ramirez, S. Nasir, Q.-H. Nguyen, W. Ensinger, S. Mafe, *Appl. Phys. Lett.* **2014**, *104*, 043703.
[60] S. Mafé, P. Ramírez, A. Alcaraz, *J. Chem. Phys.* **2003**, *119*, 8097.
[61] E. M. Nestorovich, C. Danelon, M. Winterhalter, S. M. Bezrukov, *Proc. Natl. Acad. Sci. U. S. A.* **2002**, *99*, 9789.
[62] K. Kontturi, L. Murtomäki, J. A. Manzanares, *Ionic Transport Processes*, Oxford University, Oxford **2008**.
[63] J. Cervera, B. Schiedt, R. Neumann, S. Mafe, P. Ramirez, *J. Chem. Phys.* **2006**, *124*, 104706.
[64] M. Aguilella-Arzo, J. Cervera, P. Ramirez, S. Mafe, *Phys. Rev. E* **2006**, *73*, 041914.
[65] S. Mafé, J. A. Manzanares, P. Ramirez, *Phys. Chem. Chem. Phys.* **2003**, *5*, 376.
[66] P. Aranda, J. C. Galván, B. Casal, E. Ruiz-Hitzky, *Colloid Polym. Sci.* **1994**, *272*, 712.
[67] H. C. Visser, D. N. Reinhoudt, F. de Jong, *Chem. Soc. Rev.* **1994**, *23*, 75.